# Finite element analysis of effects of soft zones on formability of laser welded advanced high strength steels

**S. K. Panda*, M. L. Kuntz and Y. Zhou**

Applications of advanced high strength steels in tailor welded blanks are a major focus to reduce vehicle weight and manufacturing cost, and to improve part performance. In the present work, formability of two types of laser welded steels in biaxial stretch forming has been studied. Laser welded blanks of the dual phase steel showed larger reduction of formability than those of high strength low alloy steel. This was due to formation of soft zones in the outer heat affected zone of dual phase steel where strain localisation and fracture occurred. Finite element simulations of dome testing incorporating local weld zone properties were able to accurately predict experimentally observed behaviour including deformation patterns and failure locations. In particular, the simulations have shown that under matching of the softened heat affected zone leads to reduced formability by localisation of strain; and that the fracture location changes from radial to circumferential plane when the flow curve of soft zone is evenly matched with the base metal. It was also concluded that the width of the soft zone has minor influence on formability during biaxial stretch forming.

**Keywords:** Advanced high strength steels, Laser welding, Formability, Stretch forming, Strain localisation, Finite element



## Introduction

In recent years, significant improvement has been made in the production of sheet metal with high formability. Low carbon steel has long been the workhorse in automotive and consumer industries because it can be stamped into inexpensive, complex shapes at high production rates. Extra deep drawing and interstitial free steels, due to their excellent formability, are currently the most widely used sheet materials for automotive stamping applications. A number of reports have been published on formability of extra deep drawing and interstitial free steels.[1–3] To address the objectives of decreased body in white weight and improved crashworthiness, steelmakers have introduced a family of steels having superior combinations of strength and formability.[4] These advanced high strength steels (AHSS) are increasingly being considered by automakers in structural, exterior, enclosure and suspension applications.

In traditional sheet metal forming processes, a one piece blank of uniform thickness is typically cut from a large sheet. However, the relatively recent trend of using tailor welded blanks (TWBs) employs two or more sheet shapes with different strength and/or thickness that are joined together to create a blank with engineered properties. The TWBs are then stamped into the final desired shape with properties tailored to fit the particular application. Along with strength and thickness, quality and coating characteristics can be optimised in areas where these properties are required.

The TWBs offer several notable benefits including reduced manufacturing costs, minimised offal and improved dimensional consistency.[5,6] The application of AHSS in TWB processes has the potential to significantly reduce part weight and improve occupant protection; however, a reduction in formability as a result of the welding process has been reported.[7–9] Advanced high strength steels have inherently higher alloying levels and, as a result, exhibit high hardenability in the weld fusion zone and high temperature heat affected zone (HAZ). Furthermore, exposure to subcritical temperatures in the outer HAZ causes tempering of the martensitic constituent resulting in local softening of the microstructure.[10] The high property gradients found in the weld region of laser welds in AHSS have been found to reduce formability compared to the parent metal.[8] In order to take full advantage of the benefits of AHSS and TWB technology, designers need to overcome the problem of reduced formability early in the design process.

The ability of a sheet metal to be worked into different shapes without flow localisation under complex conditions of loading and deformation is called formability. Flow localisation is an unstable flow where the deformation is confined to one zone of the sheet metal.

Centre for Advanced Materials Joining, Department of Mechanical Engineering 200, University of Waterloo, University Avenue West Waterloo, N2L 3G1, Waterloo, Ontario, Canada


Published by Maney on behalf of the Institute
Received 12 June 2008; accepted 18 July 2008
DOI 10.1179/136217108X343920

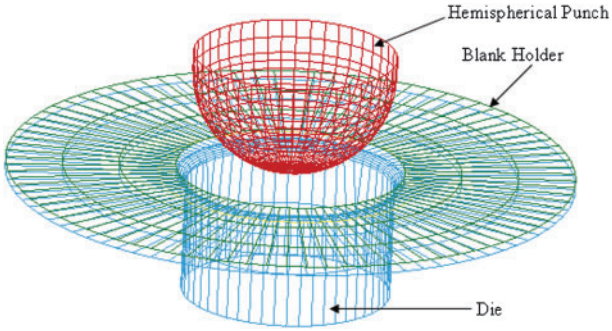


**1 Finite element modelling of tooling used in limiting dome height test**

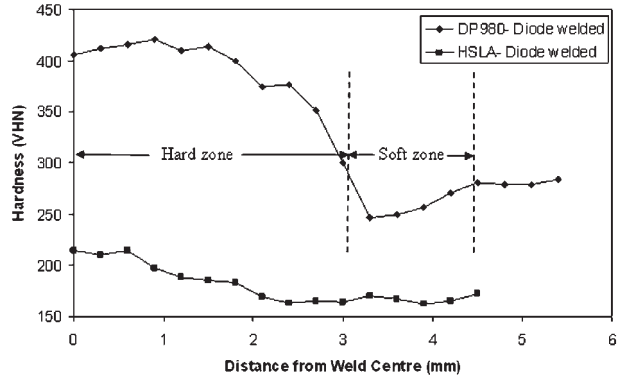


**2 Hardness profile of laser welded steels**

This is also referred to as the onset of necking, which leads to fracture on further deformation.[11] When a stamping tears during forming, the tear is a visible indication that metal has been worked beyond its prevailing forming limit. Whether or not a particular sheet of metal can be formed without failure depends on many factors such as material properties, surface conditions, blank size and shape, lubrication, press speed, blank holder pressure, punch and die design. Because of this, the source of the flow localisation problem is difficult to pinpoint and quantify. Hence, formability is an attribute that has no precise, universal meaning. With the multitude of materials, stamping designs and press conditions, there are no standard rules for improving the formability of a stamping through changes in tool design or process parameters.[12,13] Predicting failure in the manufacturing process of thin sheet metal parts is not a simple task, largely because of the complex boundary and interfacial conditions, and the difficulty of describing the neck initiation and growth behavior.[14] Therefore, evaluation of formability of sheet metals prior to manufacturing is useful for correcting failures.

If the authors restrict their attention to stretch forming, the limit of formability is associated with the onset of plastic instability, at which point the sheet locally thins catastrophically and tears. This is the behaviour characterised by the onset of localised necking of a sheet in the uniaxial tension test. In more complex sheet forming operations, multiaxial stresses and strains are imposed. Experience has shown that the limiting dome height (LDH) test, in which a clamped sheet is deformed by a spherical punch (out of plane stretching) until fracture, provides a useful measure of the forming limit for many punch stretching operations of the sort used in manufacture of automotive vehicles.[15]

Dry *et al.*[16] studied the formability of laser welded blanks by determining the weld material properties, and outlined how the weld properties were used in the finite element (FE) analysis simulation of simple small scale dome height tests. They did not found any softening in the HAZ and hence soft zone properties were neglected during FE simulations. In the present work, FE analysis was used to simulate biaxial stretch forming of two types of laser welded blanks by incorporating hard and soft zone properties. The results of the FE analysis have also been compared with actual LDH test results and are shown to accurately predict blank failure modes. Finite element analysis was performed by the commercially available LSDYNA code (version 971). LSDYNA is an explicit time integration dynamic solver which can handle material, geometrical and contact nonlinearities in solving quasi-static sheet metal forming.[17] In the Hypermesh software, the pre- and post-processors (LS-PREPOST) are integrated with LSDYNA.

## Finite element analysis

### Modelling of tooling and TWB

The tools (die, punch and blank holder) and the blank were created by surface modelling and were discretised in the preprocessor (HYPERMESH). A typical FE model of the tools used for simulation of stretch forming is shown in Fig. 1. In order to capture the details of the surfaces of the tools and blank, the surface automesh option was used.

Tools (hemispherical punch, die and blank holder) were modelled as rigid bodies to avoid deformation of the tools during stretch forming. In the present work, Belytschko–Tsay thin shell elements were used for the blank and tools because of their reduced computational time. For example, four noded Belytschko–Tsay shell elements require 30–50% less processing time than the others.[17] Adaptive mesh generation methodology was used in simulations to obtain greater accuracy. In this method, the elements are subdivided into smaller elements wherever an error indicator shows that subdivision of elements will provide improved accuracy.[17]

Variations in the post-weld microstructure and properties across the fusion zone and HAZ were modelled with a heterogeneous sheet. The microhardness profiles measured across the laser welds are shown in Fig. 2 for both DP980 and high strength low alloy (HSLA) steels. It can be seen that the hardness of the weld fusion zone and the inner part of the HAZ was higher than that of the parent sheet in both cases. This was due to supercritical heating in the fusion zone and high temperature HAZ along with high cooling rates that produced hard austenitic decomposition products. In the outer HAZ, where the peak temperature during welding was subcritical, microstructural examination showed tempering of the martensite constituent of the DP980 steel. This resulted in the formation of a soft zone at the outer edge of the HAZ. The width of the soft and hard zones of DP980 steel after laser welding depended on laser power, welding speed and welding mode, as shown in Table 1.[18] In HSLA, however, there was no martensitic phase, and as a result, no significant softening was observed after welding. To study the influence of the weld hard zone and soft zone properties

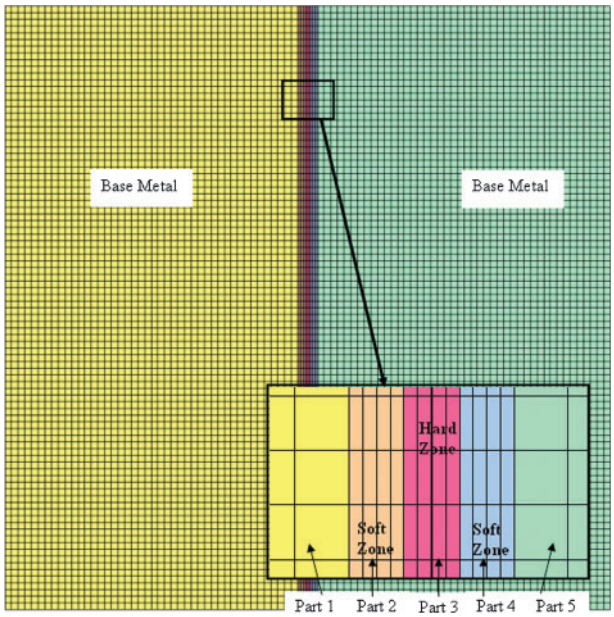


**3 Finite element modelling of laser welded blank incorporating soft and hard zones**

on the simulation results, TWBs were modelled by defining five separate regions (Fig. 3) with simple merging of the nodes. The corresponding properties/thicknesses were assigned to individual regions of the blank. The central region was the hard zone, which consisted of the fusion zone and hardened HAZ. The adjacent regions were assigned the soft zone properties. If a soft zone was not formed (as in the case of HSLA steel), the base metal properties were assigned to this region.

## Material model for tooling and blank

The blanks were considered as deformable bodies with appropriate yield criteria and stress–strain relations during non-linear plastic deformation to account for strain hardening. The yielding behaviour of the blank material was considered as per Barlat's three parameter plasticity model.[19] This model incorporates the effect of both normal and planar anisotropy in polycrystalline sheet during deformation as shown below

$$\Phi = a|K_1 + K_2|^m + a|K_1 - K_2|^m + c|2K_2|^m = 2\sigma_Y^m \quad (1)$$

where Φis yield function, $\sigma_Y$ is yield stress, $m$ is Barlat's yield exponent and it was suggested that, for body centred cubic materials, the most suitable value is six. Therefore $m=6$ has been used in the present work.

$K_1$ and $K_2$ are stress tensor invariants.

$$K_1 = \frac{\sigma_x + h\sigma_y}{2} \quad (2)$$

$$K_2 = \left[\left(\frac{\sigma_x - h\sigma_y}{2}\right)^2 + p^2\tau_{xy}^2\right]^{\frac{1}{2}} \quad (3)$$

where $\sigma_x$, $\sigma_y$ and $\tau_{xy}$ are plane stress components in orthotropic axes.

$a$, $c$, $h$ and $p$ are anisotropic material constants and these are obtained from Lankford's parameters as given below

$$a = 2 - 2\left(\frac{R_0}{1+R_0}\frac{R_{90}}{1+R_{90}}\right)^{\frac{1}{2}} \quad (4)$$

$$c = 2 - a \quad (5)$$

$$h = \left(\frac{R_0}{1+R_0}\frac{1+R_{90}}{R_{90}}\right)^{\frac{1}{2}} \quad (6)$$

$p$ is normally calculated implicitly after knowing $a$, $c$ and $h$.[19]

The stress–strain relation for strain hardening of the sheets during plastic deformation is represented by the following constitutive equation[20]

$$\sigma_y = K\varepsilon^n = K(\varepsilon_{yp} + \varepsilon^p)^n \quad (7)$$

where $\sigma_y$=flow stress, $\varepsilon_{yp}$ =strain to yield, $\varepsilon^p$=effective plastic strain, $K$ is strength coefficient and $n$ is strain hardening exponent.

The elastic strain at yield can be found from[17]

$$\varepsilon_{yp} = \left(\frac{\sigma_y}{K}\right)^{\frac{1}{n}} \quad (8)$$

The experimental values obtained for $n$, $K$, $R_0$, $R_{45}$ and $R_{90}$ in tensile tests were used to define the material parameters of the blanks. In the case of DP980, the hard weld zone material does not obey the constitutive equation.[18] The hard zone mechanical behaviour was defined from the data obtained in the longitudinal tensile tests on microtensile size specimens. It was considered as isotropic, owing to the following considerations:

(i) the hard zone was formed by heating beyond the melting point and then cooling of a narrow zone of material and hence the prior crystallographic structure would be completely removed

(ii) the width of the weld zone was too small to measure any anisotropy of properties. Hence anisotropy in that small region has been neglected by defining $R_0=R_{45}=R_{90}=1{\cdot}0$.

Experimental determination of the strength coefficient and strain hardening exponent for the HAZ was not possible. It was assumed that the softened HAZ obeys the power law of hardening during deformation. For simulation purposes, the strength coefficient and $n$ value

**Table 1 Measured width of hardened and softened zones in laser welds of DP980 steel**

| Types of laser | Welding parameters | | | Experimental softened zone width at one side, mm | Experimental hardened zone width at one side, mm |
|---|---|---|---|---|---|
| | Weld speed, m min$^{-1}$ | Laser power, kW | Beam size | | |
| Diode | 1·9 | 4 | 12×0·9 mm | 2·0 | 3·2 |
| Nd:YAG | 6·0 | 3 | 0·6 mm ø | 0·5 | 0·5 |

were obtained through a pragmatic process optimisation until the load displacement curve matched well with the experimental result (by comparing the load displacement curve obtained from both experiments and FE simulations, i.e. different combinations of the $K$ and $n$ values were tried to provide the best fit with experimental load versus displacement curve).[18] This zone was also considered to be isotropic.

### Boundary conditions

An analytical draw bead was created on the die by applying a restraining force on the blank. When the blank slides on the die, it experiences that restraining force and hence gets stretched instead of drawing in. A few trial simulations were conducted to identify the minimum required blank holding force to completely eliminate drawing in.

The friction between the blank and rigid surfaces was modelled using Coulomb's friction. The coefficient of friction between the blank and tools for conventional stretch forming was taken as 0·12 (between the blank and the punch surface)[21] and 0·23 between blank and die and blank and blank holder.[1] This reflects the use of a polyurethane sheet applied as lubricant between blank and punch during stretch forming experiments.

The die and blank holder were considered fixed entities and the punch was moved down with a velocity equal to 1000 mm $s^{-1}$ in the negative $Z$ direction, whereas in actual experiments, the punch velocity was 2 mm $s^{-1}$ in conventional stretch forming. This was conducted to reduce the simulation time. As the effect of strain rate has not been considered in defining the deformation behaviour of the materials, this would not affect the simulation results. Han *et al.*[22] found that there was a very minor change in yield strength, ultimate tensile strength (UTS) and strain hardening coefficient of dual phase (DP) and HSLA steels within the strain rate range of 0·01 to 0·0001 $s^{-1}$. Hence in these steels, the effect of strain rate during low (quasi-static) forming rates at room temperature can be neglected.

### Failure criteria

In the simulations, theoretically calculated forming limit diagrams (FLDs) are used to predict failure during deformation. An FLD or a forming limit curve is constructed by plotting the major and minor limit engineering strains. In an FLD, the limiting curve intersects the $Y$ axis (major strain axis or the plane strain line) at an intercept called $FLD_0$. In the post-processor (LS-PREPOST), $FLD_0$ is calculated using thickness and $n$ value of the sheet material. The standard Keeler Goodwin diagram[23] for a low carbon steel sheet of 1 mm thickness was taken as the reference FLD. The following equations were used to calculate the $FLD_0$ (engineering strain) for plotting the FLDs of the sheets which were used in the simulations.

If $t<2{\cdot}54$ mm,

$$FLD_0 = \frac{n}{0{\cdot}21}(23{\cdot}3 + 14{\cdot}13t) \quad (9)$$

where $t$ is sheet thickness in mm and $n$ is strain hardening coefficient of the sheet.

For failure prediction of TWBs, the thickness and $n$ value of the weaker zone were used. The cup height at the first appearance of failure/necking was used for determining the limiting dome height as shown in Fig. 4.

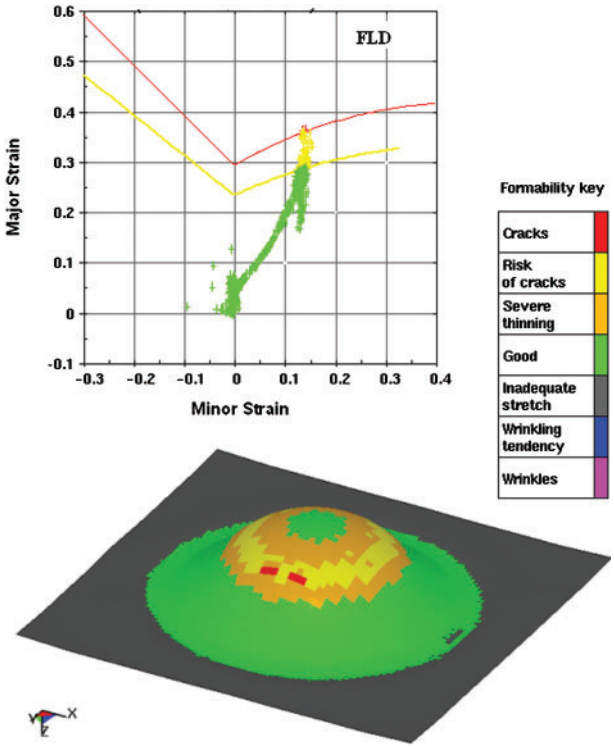


**4 Typical cup failure in finite element method (FEM) simulation of stretch forming for HSLA parent sheet**

## Experimental

### Preparation of laser welded blanks

In the present work, dual phase 980 MPa (DP980) and HSLA steel sheets were laser welded in a butt joint configuration to create blanks for formability analysis. The sheet thicknesses were 1·2 and 1·14 mm for the DP980 and the HSLA steel respectively. The as received microstructure of the DP980 used in the present work exhibited a ferrite matrix with a significant volume fraction of fine martensite laths (49·4%) decorating the grain boundaries.[8] The HSLA steel had a typical fine grained ferrite pearlite microstructure featuring fine precipitates.[8]

Laser welds were produced using high power diode and Nd:YAG power sources. The equipment consisted of a Nuvonyx ISL-4000L diode laser system (a 4 kW AlGaAs diode laser) with a laser head mounted and deployed on the arm of a Panasonic VR-016 welding robot, and a Haas HL3006D Nd:YAG laser system (a 3 kW Nd:YAG laser) with fibre optic beam delivery. Two similar sheets (i.e. DP980-DP980, or HSLA-HSLA) were clamped in a fixture and butt welded together with the weld line oriented transverse to the rolling direction. The welding process was conducted at welding speeds of 1·9 and 6·0 m $min^{-1}$ in order to achieve full penetration welds with the diode and Nd:YAG lasers respectively. The beam characteristics of both power sources are summarised in Table 1.

### Tensile tests

Tensile tests were carried out on specimens of parent metal sheets machined as per ASTM standard E8M specification.[24] The specimens were tested along three directions, with the tensile axis being parallel (0°), diagonal (45°) and perpendicular (90°) to the rolling

direction of the sheet. A constant cross head speed of 2 mm $min^{-1}$ was employed in all cases. The standard tensile properties 0·2% offset yield strength (YS), ultimate tensile strength, elongation percentage, strain hardening coefficient $n$ and strength coefficient $K$ were determined. The strain hardening behaviour of the sheets can be described by using the constitutive equation (7).[20]

Though anisotropy was not expected to have a significant influence on formability in stretch forming, the values of anisotropic parameters of the materials were important for accurate simulation of the process using FEM. It was particularly important in the present study as the sheet materials had high anisotropy (both normal and planar). The Barlat's 3-parameter yield criterion[19] incorporates the effect of anisotropy on the yielding behaviour of the material. The plastic strain ratio $R$ of the parent materials was evaluated using specimens made to ASTM E517 specification.[24]

The $R$ value was evaluated in three directions and the normal anisotropy was calculated by using the standard formula[23]

$$\overline{R} = \frac{R_0 + 2R_{45} + R_{90}}{4} \tag{10}$$

where the subscript indicates the orientation of the specimen axis with respect to the rolling direction.

Sub size tensile specimens were cut from the laser welded samples for conducting the tensile tests in transverse directions on the TWBs according to ASTM E8M standard.[24] The tensile tests were conducted at a constant cross head speed of 2 mm $min^{-1}$ until fracture. Transverse tests were used to ensure that the weld does not crack during deformation. The load displacement data was also used to evaluate the $K$ and $n$ values of the soft zone for the DP steel. The detailed procedure is given elsewhere.[18]

## Biaxial stretch forming tests

The biaxial stretch forming tests were carried out according to the procedure suggested by Hecker[25] using a hemispherical punch with a 101·6 mm diameter on a double action hydraulic press. Square specimens $180 \times 180$ mm were cut from the laser welded blanks. A 132 mm diameter circular draw bead was provided on the dies to restrict the flow of metal from the flange region into the die and to ensure that only the portion within the die opening was deformed by the punch. The specimens were placed on the lower die such that weld line was at the middle of the die opening. Since the specimen width is greater than the draw bead diameter, it ensures complete clamping of the blank at the drawbead and hence samples were subjected to biaxial tensile stresses. All the tests were conducted with application of polyurethane sheet and lubrication in between punch and sheet at a punch speed of 2 mm $min^{-1}$. An optimum blank holing force was applied on the upper die so that there will be no drawing in of the blank from the flange region. The experiments were stopped when a visible neck or initiation of fracture was observed on the specimens.

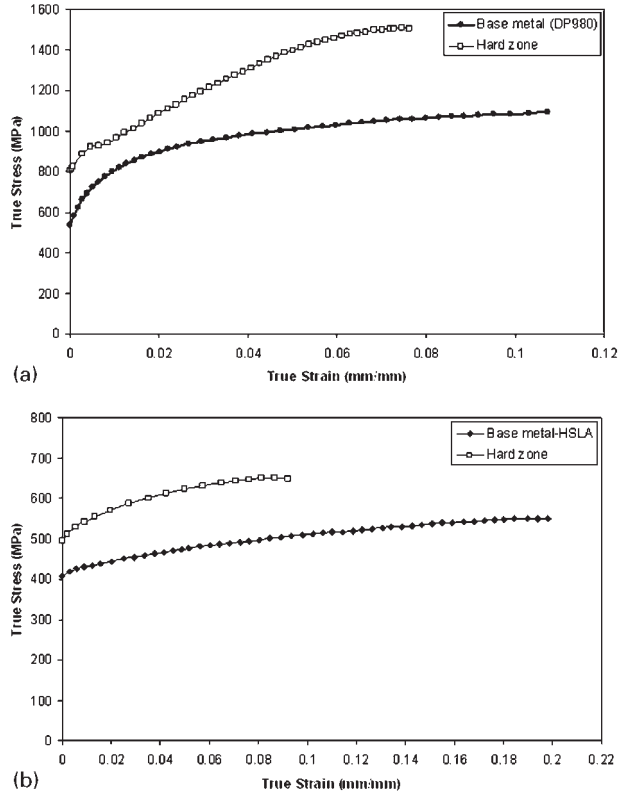


*a* DP980 steels; *b* HSLA steels

**5 True stress–true strain curve for base metal and weld zone**

# Results and discussion

## Tensile testing

The standard tensile properties 0·2% offset YS, UTS, elongation percentage, strain hardening exponent $n$, strength coefficient $K$ and anisotropic parameters ($R_0$, $R_{45}$ and $R_{90}$) of the parent AHSS sheets are given in Table 2. It is observed that the DP980 has a significantly higher YS and UTS compared to the HSLA, but it also has a lower total elongation. The morphology of the martensite in the ferrite matrix of the DP980 induces a higher UTS/YS and lower ductility (elongation percentage) as compared to the HSLA.

The HSLA possessed a higher $n$ value (0·18) and was expected to have better stretchability than the DP980 ($n$=0·14). The strain hardening exponent describes the ability of the material to distribute strain uniformly during plastic deformation before localised necking or excessive thinning occurs, hence a higher strain hardening exponent is an indication of enhanced stretchability.[26]

**Table 2 Mechanical properties of DP980 and HSLA steels**

| | | | | | | Lankford parameters | | | |
|---|---|---|---|---|---|---|---|---|---|
| Grade and sheet thickness | YS, MPa | UTS,MPa | Elongation, % | *K*,MPa | *n* value | $R_0$ | $R_{45}$ | $R_{90}$ | $\bar{R}$ |
| DP980 (1·20 mm) | 533·8 | 979·1 | 15·2 | 1510 | 0·14 | 0·80 | 0·93 | 0·85 | 0·88 |
| HSLA (1·14 mm) | 381·7 | 440·5 | 33·5 | 719·12 | 0·18 | 0·75 | 1·25 | 1·11 | 1·09 |

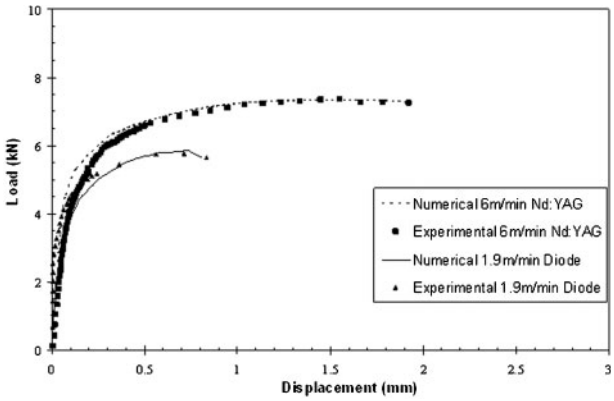


**6 Comparison of numerical and experimental uniaxial tensile test load displacement curves[15]**

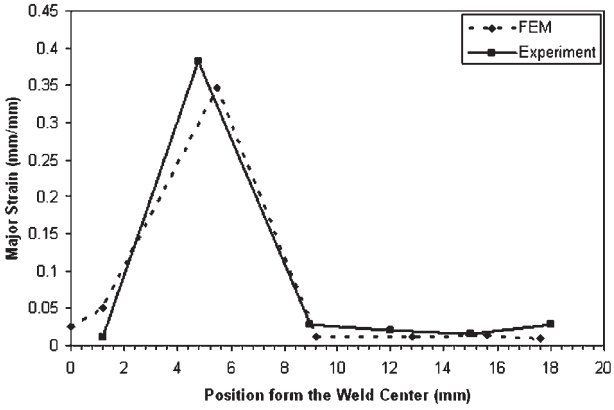


**7 Major strain distribution in diode laser welded tensile specimen of DP980: at welding speed of 1·9 mm min$^{-1}$ (Ref. 15)**

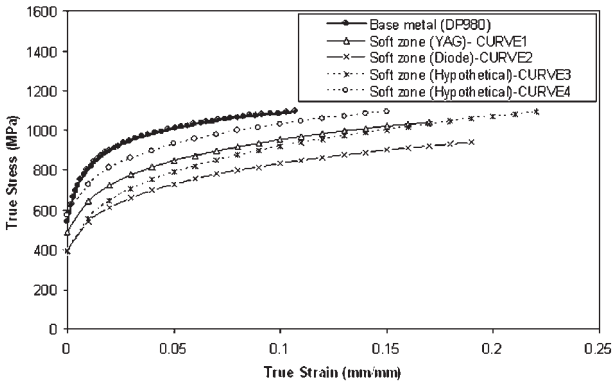


**8 True stress–true strain curves (flow curves) of soft zone compared to base metal (curves 1 and 2 are estimated; curves 3 and 4 are hypothetical)**

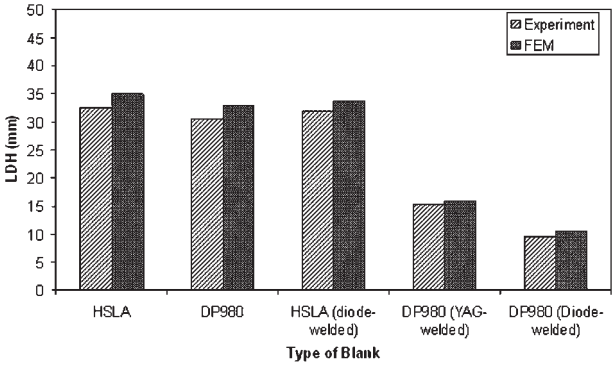


**9 Experimental and FE results of limiting dome height of parent and laser welded blanks**

The average anisotropy (normal anisotropy) of the HSLA was higher than the DP980. The $R$ value of a steel sheet is an indication of the resistance to failure due to thinning during deep drawing. Hence, the drawability of the HSLA steel sheet was expected to be relatively higher than the DP980 steel. However, since the value of normal anisotropy of both the DP980 and the HSLA sheets was close to 1·0, the overall drawability of these steels was expected to be low since a higher normal anisotropy is an indication of improved drawablity.

A comparison of typical true stress–true strain curves between the base metal and the weld hard zone for both the HSLA and DP980 is shown in Fig. 5. In both cases, the YS and UTS were higher and the ductility was lower in the weld hard zone. There was a greater increase in strength in the DP980, which has a higher alloy content, and thus increased hardenability (Fig. 2). The observed true stress–true strain behaviour of the DP980 weld hard zone did not follow the power law of hardening; however, in the HSLA weld hard zone the strain hardening exponent was 0·157. The HSLA base metal had a strain hardening coefficient of 0·18, thus the ductility of the weld hard zone was considerably lower.

In transverse tensile tests, the fracture invariably occurred within the soft zone of the weld in the DP980. During tensile testing it was found that strain was localised in the soft zone.[18] A typical comparison of experimental and simulated load displacement curves is shown in Fig. 6. The major strain distribution on the tensile sample was measured and compared with the simulation results for validation (Fig. 7).[18] These results were used to find the $K$ and $n$ values of the soft zone, which were then used to evaluate tailor welded blank formability in the LDH test. The $K$ and $n$ values of the soft zone for both the diode and Nd:YAG laser specimens obtained by the above procedure is given in Table 3. These material constants were used to define the flow curves of the soft zone, which are shown in Fig. 8. In the case of the HSLA, there was no soft zone formation, hence ductility of the welded blank was not significantly reduced in transverse tensile testing.

**Table 3 $K$ and $n$ values of softened zone as compared to base metal used in numerical simulations**

| | | Softened zone | | | |
|---|---|---|---|---|---|
| Properties | Base metal | Nd:YAG laser (curve 1) | Diode laser (curve 2) | Hypothetical (curve 3) | Hypothetical (curve 4) |
| $n$ value | 0·14 | 0·17 | 0·19 | 0·22 | 0·15 |
| $K$ value, MPa | 1510 | 1408 | 1290 | 1525 | 1455 |

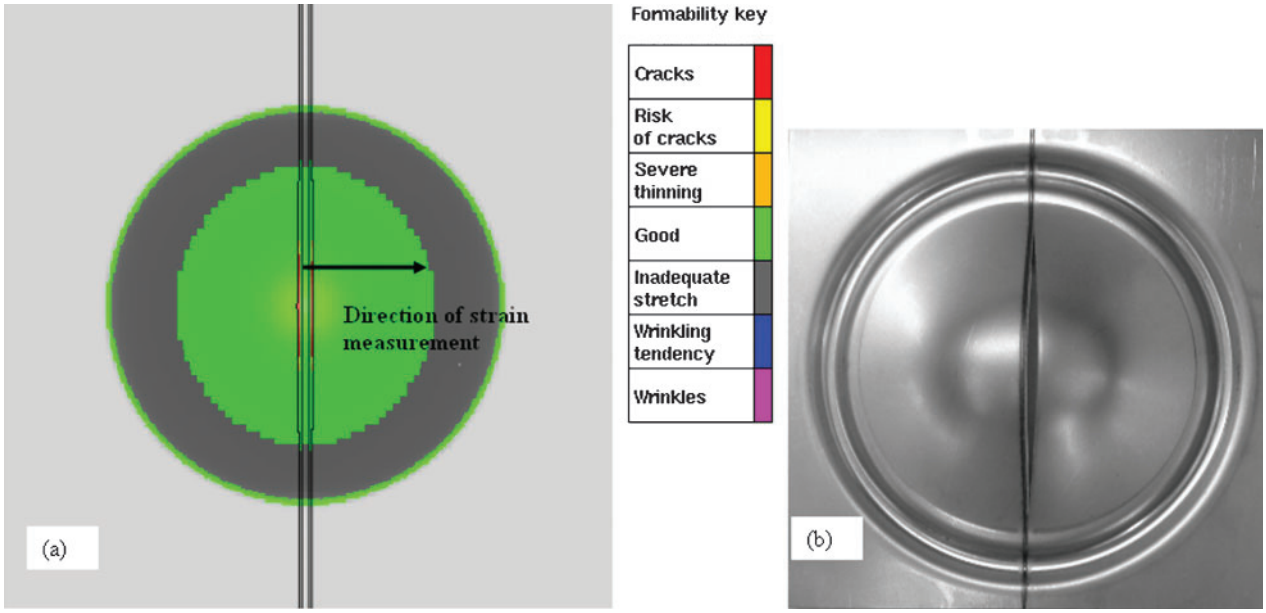


*a* prediction form simulation; *b* experimental observation

**10 Fracture in soft zone of deformed DP980 laser welded blank**

## Limiting dome height

The experimental and simulated LDH results for the parent metal and welded blanks are shown in Fig. 9. The LDH for the DP980 parent metal was lower than that of the HSLA. This was due to higher strain hardening of the HSLA, which increased formability in stretch forming. There was a slight decrease in the LDH of the HSLA welded blanks. Conversely, there was a major reduction in the LDH of the DP980 laser welded blanks. This was due to the presence of the soft zone in the HAZ of the welded DP980 steel, where strain localisation occurred. Failure invariably occurred along the soft zone, running parallel with respect to the weld line (Fig. 10).[8] In the HSLA, there was no soft zone and fracture occurred across the weld, with the reduction in formability resulting from hardening in the fusion zone and HAZ (Fig. 11). However, there was no significant difference in LDH between diode and Nd:YAG laser welded HSLA steel sheets (31·8 and 32·9 mm respectively). This implies that any small change in width of the hard zone within a relatively large deformation region does not have major influence on formability. In all cases, the FEM prediction of LDH and fractured location matched well with experimental values for laser welded blanks.

## Strain distributions

To better understand the forming issues of TWBs, the predicted major strain from the FEM results was plotted with distance from the pole (Fig. 12). The strain distribution pattern is important in assessing the

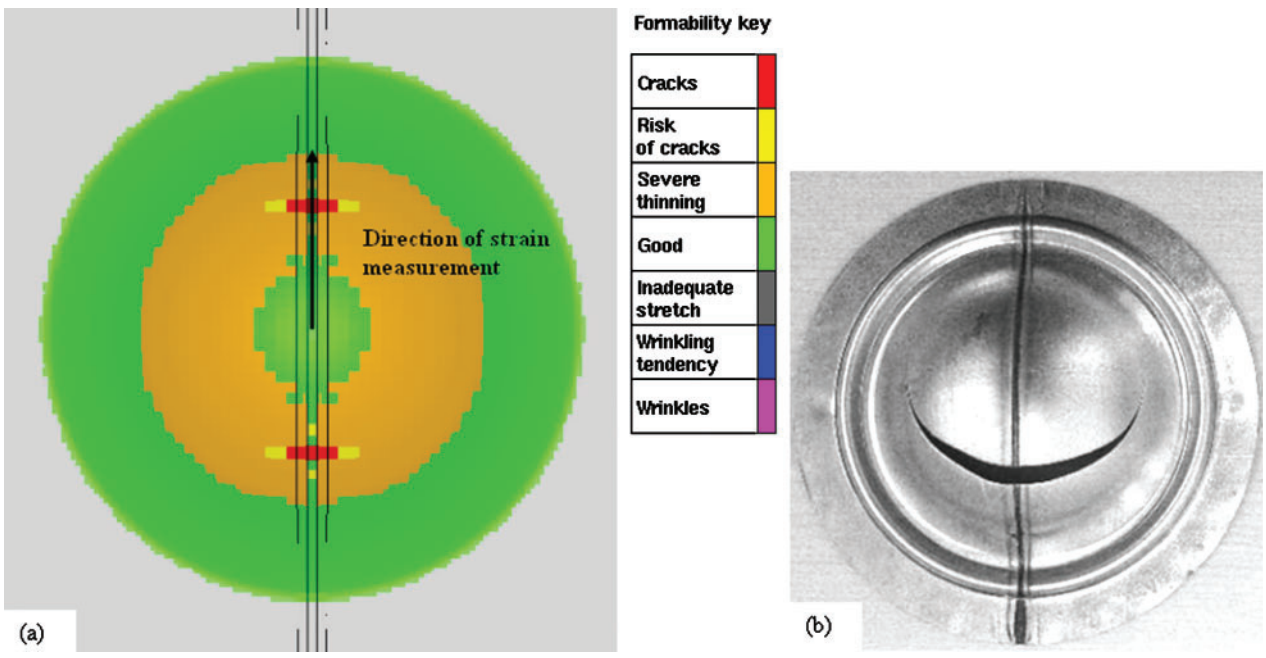


*a* prediction form simulation; *b* experimental observation

**11 Fracture across weld of deformed HSLA laser welded blank**

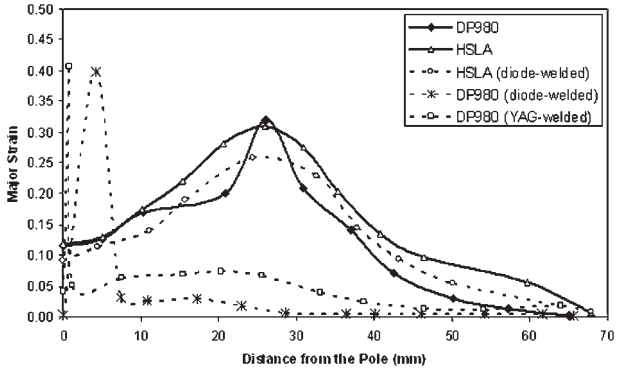


**12 Finite element simulated strain distributions along lines shown in Figs. 14 and 15 for HSLA and DP980 laser welded blanks**

formability of the blank with the FLD. The laser welded blank is symmetric about the weld line, so only one side of the strain distribution is shown in the figure. The strain distribution was measured across the fracture location (Fig. 12). In the parent sheet, the strain gradient of the DP980 steel was higher in comparison to the HSLA. This was due to the higher strain hardening of the HSLA, which increases uniform deformation. The resulting LDH of the HSLA was higher compared to the DP980.

In the laser welded blanks, even higher strain gradients were observed in the DP980 specimens. There were peaks in major strain within the soft zone and close to the pole, where fracture occurred. There was negligible deformation (major strain $<5\%$) in the hard region at the pole, and in the base metal away from pole. This indicated that the formability decreased due to strain localisation in the soft zone during deformation. The LDH of the DP980 welded blanks was higher in Nd:YAG case. Thus, there was more deformation in the base metal region of the Nd:YAG welded DP980 blank compared to diode welded blank as shown in Fig. 12. The major strain distribution in the HSLA welded blank was more uniform. There was a clear peak

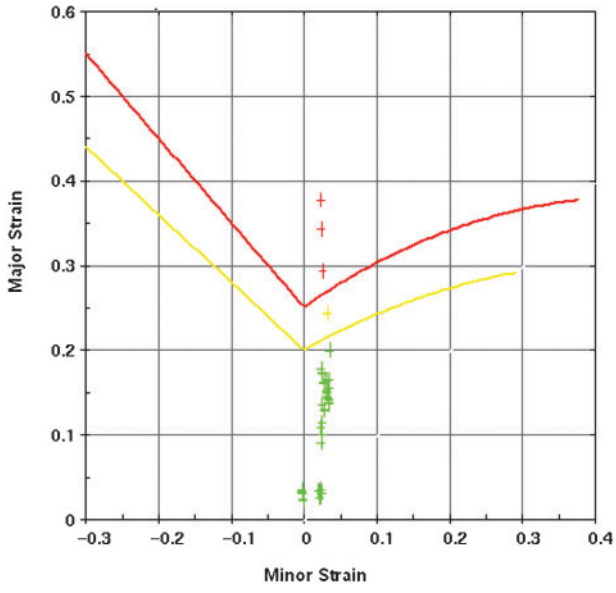


**13 Strain state in FLD of deformed DP980 laser welded blank**

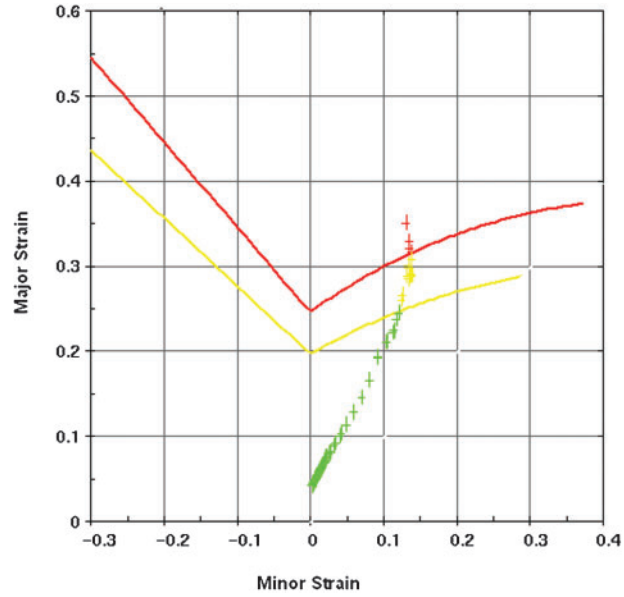


**14 Strain state in FLD of deformed HSLA laser welded blank**

away from the weld, corresponding to the absence of a soft zone in the HAZ.

The predicted major and minor strain at fracture of the stretched dome was imposed on the FLD for the welded blanks. The FLD was calculated by the thickness and $n$ value of the fractured region, i.e. the soft region for the DP980 and the hard weld region for the HSLA. A plane strain state was observed in the case of the DP980 welded blank (Fig. 13). Owing to the presence of the weaker soft zone, a plane strain state occurred from the initiation of deformation and induced earlier failure. In the case of the HSLA welded blank, the strain states tended more towards biaxial stretching (Fig. 14) which resulted in a higher forming limit strain and increased LDH.

Finite element analysis of welded DP980 blanks was used to define the independent effects of width and properties. The FE model was developed assuming a constant hard zone width of 2·0 mm and varying soft zone widths (0, 0·5, 1·5 and 2·0 mm respectively). Material flow properties were uniformly assigned across the zones. The LDH showed an immediate decrease with the formation of a soft zone (i.e. width>0). With increasing soft zone width, the LDH was nearly constant, as shown in Fig. 15. To characterise the effect

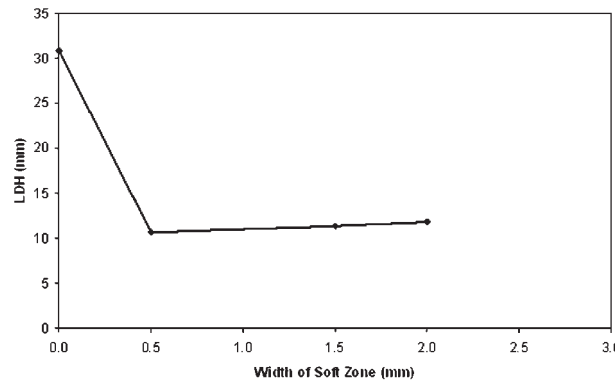


**15 Variation of predicted limiting dome height with width of soft zone**

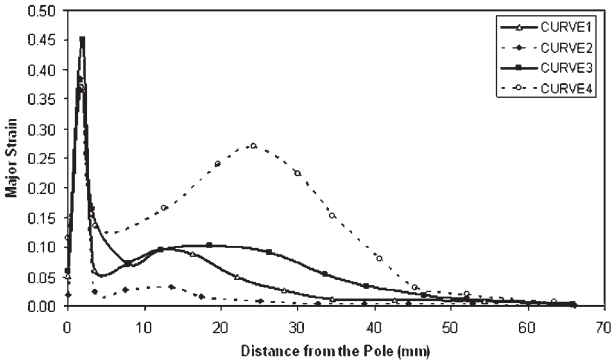


**16 Finite element strain distribution in deformed samples for four different soft zone property conditions**

of softening on formability and strain distribution, the LDH was simulated for four levels of soft zone properties by assigning different flow curves: i.e. curves 1–4 (Fig. 8). Curves 1 and 2 represent the respective soft zone flow curves determined for the diode and Nd:YAG laser welded blanks. To cover a wide range of under-matched conditions of the soft zone, two more hypothetical curves, curves 3 and 4 were assumed with corresponding $K$ and $n$ values, as shown in Table 3. In all of the above simulations, fracture occurred in the soft zone. Figure 16 shows the strain distribution for different under matched conditions. The strain levels were lowest in case of curve 2 (in diode welded case), which represented the most severe under matched condition. There was higher strain in the deformed samples in case of curve 3 compared to curve 2. This is due to higher $n$ value, which promoted delayed necking and improved strain distribution in the adjacent base metal. The strain levels on the deformed samples were the highest in case of soft zone properties assigned by curve 4, which was close to the base metal flow curve. Curves 3 and 4 had the same UTS and curves 2 and 3 had the same yield strength, however, there were different strain distributions and LDHs (Fig. 17) for all of the above conditions. Hence, it was the complete nature of the soft zone flow curve and its relative under matching with the base metal which determined the formability. When the soft zone was assigned the same flow properties as that of the base metal, the fracture occurred across the weld with the deformation pattern shown in Fig. 18. It can be observed that when the soft zone strength was evenly matched with the base metal,

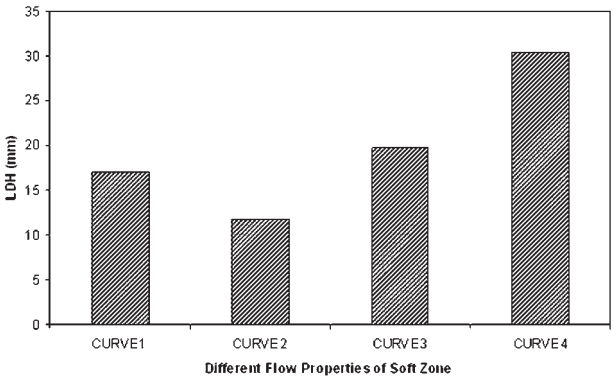


**17 Predicted effect of soft zone flow curve on limiting dome height of DP980 laser welded blanks**

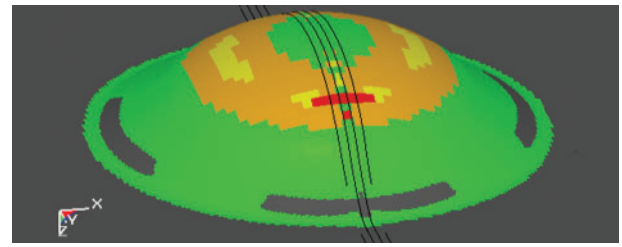

**18 Predicted deformation pattern of stretch formed specimen when flow properties of soft zone are same (even matched) as base metal**

there was a good amount of deformation in the dome with no strain localisation in the soft zone.

## Conclusions

1. The HSLA had a higher $n$ value compared to the DP980 steel. Hence it had higher formability in stretch forming. Strain distribution was more uniform in the HSLA steel compared to the DP980 steel in the LDH test. This was due to higher $n$ value of the HSLA steel.
2. Limiting dome heights of welded blanks were lower than those of the respective parent metals. The reduction in formability was larger in case of the DP980 welded blanks. This was due to strain localisation in the soft zone and a failure mode that was close to the plane strain condition.
3. The limiting dome height (formability) of a welded dual phase (980 MPa) blank that exhibits a soft zone depends on the nature of the flow properties (both $K$ and $n$ values) of the soft zone compared to the base metal. The limiting dome height will approach that of the parent monolithic sheet and the fracture location shifts away from the pole (and propagates across the weld rather than parallel to it in the soft zone) when the flow properties of the soft zone are evenly matched to the base metal.

## References

1. A. K. Gupta and D. R. Kumar: *J. Mater. Process. Technol.*, 2006, **172**, 225–237.
2. D. R. Kumar: *J. Mater. Process. Technol.*, 2002, **130–131**, 31–41.
3. Z. Wang and X. Wang: *J. Mater. Process. Technol.*, 2001, **113**, 659–661.
4. L. A. L. de Lacalle, A. Lamikiz, J. Munoa, M. A. Salgado and J. A. Sanchez: *Int. J. Adv. Manuf. Technol.*, 2006, **29**, 49–63.
5. B. Kinsey, Z. Liu and J. Cao: *J. Mater. Process. Technol.*, 2000, **99**, 145–153.
6. W. Waddell, S. Jackson and E. R. Wallach: 'The influence of the weld structure on the formability of laser welded tailored blanks', Technical paper no. 982396, SAE, Washington, DC, 1998.
7. N. Sreenivasan, M. Xia, S. Lawson and Y. Zhou: *J. Eng. Mater. Technol.*, 2008, **130**.
8. M. Xia, N. Sreenivasan, S. Lawson and Y. Zhou: *J. Eng. Mater Technol.*, 2007, **129**, 446–452.
9. M. P. Miles, J. Pew, T. W. Nelson and M. Li: *Sci. Technol. Weld. Join.*, 2006, **11**, 384–388.
10. M. I. Khan, M. L. Kuntz and Y. Zhou: *Sci. Technol. Weld. Join.*, 2008, **13**, 294–304.
11. W. Johnson and P. B. Mellor: 'Engineering plasticity', 110–114; 1975, London, Van Nostrand Reinhold Company.
12. P. B. Mellor: *Int. Met. Rev.*, 1981, **1**, 1–20.
13. K. P. Rao and W. M. Sing: *Int. J. Mech. Sci.*, 2000, **42**, 451–472.
14. D. Lee and F. Zaveri: *Int. J. Mech. Sci.*, 1982, **24**, 157–173.
15. A. K. Ghosh and S. S. Hecker: *Metall. Trans. A*, 1975, **6A**, 1065–1073.
16. D. Dry, W. Waddell and D. R. J. Owen: *Sci. Technol. Weld. Join.*, 2002, **7**, 11–18.

17. J. O. Hallquist: LS-DYNA keyword user's manual version 971, 2003.
18. S. K. Panda, N. Sreenivasan, M. Kuntz and Y. Zhou: *J. Eng. Mater. Technol*., 2008, **130**.
19. F. Barlat and J. I. Lian: *Int. J. Plast.*, 1989, **5**, 51–56.
20. G. E Dieter: 'Mechanical metallurgy', 283–292; 1988, London, McGraw Hill.
21. A. K. Ghosh: *Int. J. Mech. Sci.*, 1977, **19**, 457–470.
22. K. Han, C. J. Van Tyne, and B. S. Levy: *Metall. Trans. A*, 2005, **36A**, 2379–2384.
23. W. F. Hosford and R. M. Caddell: 'Metal forming: mechanics and metallurgy'; 2007, New York, Cambridge University Press.
24. 'Metals test methods and analytical procedures', E8M03, ASTM, Philadelphia, PA, USA, 1999.
25. S. S. Hecker*: Met. Eng. Q*., 1974, **14**, 30–36.
26. S. P. Keeler and W. A. Backofen: *Trans. ASM*, 1963, **56**, 25–48.